Multicomponent Diffusion and Convection in Capillary Structures

A previously developed method (Sotirchos and Burganos, 1988) for studying isobaric multicomponent diffusion in a class of capillary networks is extended for application to the problem of convection and diffusion of gaseous mixtures in porous media. The method is used to develop flux models for nonisobaric transport in capillary structures, which are then compared with corresponding "three-parameter" dusty-gas models. Results for discrete and continuous pore size distributions show that the predictions of the developed flux models depend strongly, both qualitatively, and quantitatively, on the procedure used to average the dusty-gas model equations for a single pore over the pore-size distribution.

Stratis V. Sotirchos
Department of Chemical Engineering
University of Rochester
Rochester, NY 14627

Introduction

In a previous article (Sotirchos and Burganos, 1988), the problem of multicomponent diffusion of gases in pore networks under isobaric conditions was investigated. The capillary structures considered in that study were visualized as consisting of cylindrical pore segments arranged around the bonds of a two- or three-dimensional lattice, with two-dimensional capillary structures understood as embedded in a slice of the porous medium. The isobaric form of the dusty-gas model equations (Deriagin and Bakanov, 1957; Mason et al., 1967; Mason and Malinauskas, 1983) was used to describe the diffusion process in each pore segment, and local analysis was employed to develop diffusion flux expressions in the capillary network. Macroscopic diffusion fluxes were obtained by averaging, over the pore size and pore orientation distributions, the contributions of all pores lying in a statistically representative part of the network whose characteristic size was much smaller than the length scale associated with significant macroscopic concentration changes. In other words, it was assumed that in the smallest domain that could be considered statistically representative of the pore network, the concentrations of the diffusing species could be considered approximately constant.

Past approaches for developing multicomponent flux expressions for capillary structures (e.g., Feng and Stewart, 1973) were based on inverting the dusty-gas model equations for a single pore, that is, writing them in explicit form for the fluxes, and averaging the n^2 elements of the diffusion coefficient matrix (for a multicomponent mixture of n gaseous species) over the pore size and pore orientation distributions. The approach used by Sotirchos and Burganos (1988) exploited the special structure of the dusty-gas model equations and employed a sequence of matrix manipulations based on eigenvalue-eigenvector analysis to decompose the dusty-gas model equations, as written for a single pore, into a set of n independent flux expressions for n auxiliary species whose concentration gradients and fluxes were pore size independent, linear combinations of the concentration gradients and fluxes of the n species of the multicomponent mixture. The diffusion coefficient for each auxiliary species was then averaged over the pore size and orientation distributions by applying the smooth field approximation (Jackson, 1977) to the original network or to an equivalent pore network obtained through application of the effective medium theory (Kirkpatrick, 1973) for resistor networks (SFA and EMT-SFA flux models, respectively).

The special structure of the multicomponent flux expressions derived by Sotirchos and Burganos (1988) made possible their direct comparison with the "two-parameter" dusty-gas model for isobaric diffusion in porous media which makes use of effective, concentration-independent diffusion coefficients for binary and Knudsen diffusion. The comparison showed that the rigorous multicomponent flux model could be approximated satisfactorily by the "two-parameter" dusty-gas model provided that the same averaging procedure was used to obtain the effective diffusion coefficients of the n auxiliary species (appearing in the rigorous model) and the effective binary and Knudsen diffusion coefficients (appearing in the "two-parameter" flux model). This is a finding of immense importance since, in contrast to the effective coefficients of the n auxiliary species, the effective binary and Knudsen diffusion coefficients that appear in the "two-parameter" dusty-gas model do not depend on the concentrations of the reacting species and, consequently, do not have to be updated every time the concentration data in the capillary structure are altered, spatially or temporally.

Many gas-solid reactions, both catalytic and noncatalytic, are

accompanied by considerable volume change (Froment and Bischoff, 1979), which can lead to large pressure gradients in the interior of the porous medium and, on that account, to appreciable contribution of viscous flow to the total mass-transport flux in the porous medium. A typical example is offered by solid decomposition reactions, like the calcination of limestones and dolomites, where under some reaction conditions, viscous flow may be the dominant mode of transport of the gaseous products through the porous structure formed in the course of the reaction. Multicomponent diffusion in the presence of significant total pressure gradients may be described using a "three-parameter" variant of the dusty-gas model, which accounts for viscous flow through the use of an average permeability coefficient in D'Arcy's law (Chen and Rinker, 1979; Mason and Malinauskas, 1983). Another alternative is to use the Feng and Stewart model for nonisobaric diffusion, which is obtained by integrating the nonisobaric dusty-gas equations for a single pore over the pore sizes and pore orientations, assuming smooth microscopic concentration and pressure fields.

The extension of the eigenanalysis procedure of Sotirchos and Burganos (1988) to the more general problem of multicomponent diffusion under nonisobaric conditions is the subject of my paper. A general method for developing flux models for nonisobaric multicomponent diffusion is presented. The method is employed to construct flux models using the SFA and EMT-SFA procedures introduced in previous papers (Burganos and Sotirchos, 1987; Sotirchos and Burganos, 1988), which are then compared with the corresponding "three-parameter" dusty-gas models.

Dusty-Gas Model Equations for a Single Pore and Flux Expressions

Under nonisobaric conditions, the dusty-gas model equations in a single pore of radius r have the form (Jackson, 1977)

$$-\frac{1}{RT}\left(\nabla p_i + \frac{x_i B p}{\mu D_{Ki}}\nabla p\right) = \sum_{j\neq i}\frac{x_j \underline{N}_i - x_i \underline{N}_j}{\mathcal{D}_{ij}} + \frac{\underline{\mathbf{N}}_i}{D_{Ki}} \qquad (1)$$

where p is the total pressure of the mixture, n is the number of species in the mixture, x_i is the mole fraction of species i, p_i is the partial pressure of species i, $\underline{N}_i$ is the molar flux of species i, $\mathcal{D}_{ij}$ is the binary diffusion coefficient of species i and j, D_{Ki} is the Knudsen diffusivity of species i in the pore, and B is the permeability of a single pore (in the sense of D'Arcy's law). We have that

$$D_{Ki} = \frac{2}{3}\left(\frac{8RT}{\pi M_i}\right)^{1/2} r = Q_i r;\ B = \frac{r^2}{8} \qquad (2a, b)$$

with Eq. 2b following from the solution of the classical Poiseuille problem for flow in a tube of circular cross-section (Bird et al., 1960). Equation 1 is usually obtained by assuming that the total fluxes of the gaseous species in the pore are made up of additive viscous and diffusive contributions, i.e., for species i,

$$\underline{N}_i = \underline{N}_i^D + \underline{N}_i^V \qquad (3)$$

The viscous contributions are predicted by the equations

$$\underline{N}_i^V = -\frac{x_i B p}{\mu RT}\nabla p \qquad (4)$$

while the diffusive fluxes satisfy

$$-\frac{1}{RT}\nabla p_i = \sum_{j\neq i}\frac{x_j \underline{N}_i^D - x_i \underline{N}_j^D}{\mathcal{D}_{ij}} - \frac{\underline{\underline{N}}_i^D}{D_{Ki}} \qquad (5)$$

Equations 1, 3, 4, and 5 can also be used to describe convection and diffusion in a porous medium by using effective values for the binary and Knudsen diffusivities and the permeability: $\mathcal{D}_{ij,e}$, $D_{Ki,e}$, and B_e, respectively. It is usually assumed that

$$\mathcal{D}_{ij,e} = S_1 \mathcal{D}_{ij};\ D_{Ki,e} = \mathrm{S}_2 Q_i \qquad (6a, b)$$

With this assumption the dusty-gas model for a porous medium contains only three parameters, namely S_1, S_2, and B_e, which, hopefully, are determined only by the structure of the porous medium.

The dusty-gas model equations for a single pore (Eq. 1 or Eqs. 3, 4 and 5) were used by Johnson and Stewart (1965) and Feng and Stewart (1973) to formulate a class of flux models for pore networks, which offer considerable flexibility in the description of the pore system. The porous medium is visualized as a network of crosslinked cylindrical pores of known orientation and radius distributions. Flux expressions for the porous medium are obtained by integrating the diffusive and viscous contributions of a single pore over all pore sizes and orientations. Since the diffusive and viscous fluxes in the individual pores are determined by the microscopic concentration and pressure fields in the pore network, it is assured that the pore network is thoroughly crosslinked so that the microscopic concentration and pressure field coincide with the macroscopic ones. This assumption is what Jackson (1977) calls the smooth field approximation, and for pore k with direction vector $\underline{n}_k$ and pressure gradient for species i ∇p_{ik}, it is mathematically expressed as

$$\nabla p_{ik} = (\underline{n}_k \cdot \nabla p_i)\underline{n}_k \qquad (7)$$

with ∇p_i being the macroscopic pressure gradient for species i.

The diffusive fluxes for a single pore are integrated over all orientations and radii by first rewriting Eq. 5 in an explicit form for the fluxes. For pore k, Eq. 5 becomes

$$\underline{N}_{ik}^D = -\sum_j F_{ij}(p, \mathrm{x}, r_k)\nabla p_{jk} \qquad (8)$$

Integrating Eqs. 4 (written for pore k) and 8 over all pore sizes and orientations and using Eq. 3, the Feng and Stewart flux model for an isotropic pore system (or through orientational averaging) becomes

$$\underline{N}_i = -\sum_j F_{ij,e}(p, \mathrm{x})\nabla pj - \frac{x_i B_e p}{\mu RT}\nabla p \qquad (9)$$

with

$$F_{ij,e} = \frac{1}{3}\int_r F_{ij}\epsilon(r)dr;\ B_e = \frac{1}{24}\int_r r^2\epsilon(r)dr \qquad (10a, b)$$

$\epsilon(r)dr$ is the pore volume that belongs to pores in the range $(r, r + dr)$ including overlapping with smaller pores. In contrast to the "three-parameter" dusty-gas model, the Feng and Stewart flux model is parametrically determined only by the

pore size distribution. However, the computation of the n^2 matrix elements, F_{ij}, and of their effective values, $F_{ij,e}$, must be repeated at each set of pressure and composition values. Moreover, the form of the above flux model does not provide any insight into its relationship with the simple "three-parameter" dusty-gas model, nor does it suggest a procedure for the estimation of the adjustable parameters of the latter for a solid of known pore-size distribution. Its validity is restricted to pore networks that satisfy the smooth field approximation (Eq. 7), which for an arbitrary capillary structure violates the mass balance equations at the points where pores of different size converge.

Eigenvector-Eigenvalue Analysis of the Dusty-Gas Model Equations for Diffusion and Convection

Eigenvector-eigenvalue analysis is used to decompose the dusty-gas model equations for a single pore into a set of n single "species" diffusion problems, whose partial pressure gradients and fluxes are linear, pore-size-independent combinations of the gradients and fluxes of the actual species. The development of the procedure makes use of material introduced in Sotirchos and Burganos (1988), and the reader is advised to consult that publication before proceeding further.

Multiplying the ith equation in Eq. 1 by $\alpha_i = Q_i/Q^*$ (with Q^* being some reference quantity) and writing the result in matrix form, we obtain that

$$-\frac{1}{RT}(\boldsymbol{A}\nabla\boldsymbol{p} + \boldsymbol{b}\nabla p) = \left(\boldsymbol{B} + \frac{1}{Q^*r}\boldsymbol{I}\right)\underline{\boldsymbol{N}} \tag{11}$$

where

$$\boldsymbol{A} = \mathbf{diag}\ (\alpha_i;\ i = 1, \ldots, n) \tag{12}$$

$$\boldsymbol{b} = \frac{Bp}{\mu}\left[\frac{\alpha_i x_i}{D_{Ki}};\ i = 1, \ldots, n\right]^T \tag{13}$$

The elements of matrix $\boldsymbol{B}$ are given by the equations

$$B_{ij} = \frac{-\alpha_i x_i}{\mathcal{D}_{ij}},\ i \neq j;\ B_{ii} = \alpha_i \sum_{j \neq i} \frac{x_j}{\mathcal{D}_{ij}} \tag{14}$$

As seen from Eq. 14, the elements of $\boldsymbol{B}$ are independent of the size of the pores; consequently, this must also be true for its eigenvectors, eigenrows, and eigenvalues, z_i, y_i, and λ_i. Let $\boldsymbol{Z}$ be the matrix composed of the eigenvectors of matrix $\boldsymbol{B}$. Since $\boldsymbol{B} = \boldsymbol{Z}\boldsymbol{\Lambda}\boldsymbol{Z}^{-1}$, with $\boldsymbol{\Lambda} = \mathbf{diag}\ (\lambda_i;\ i = 1, \ldots n)$, Eq. 2 may then be written as

$$-\frac{1}{RT}(\boldsymbol{Z}^{-1}\boldsymbol{A}\nabla\boldsymbol{p} + \boldsymbol{Z}^{-1}\boldsymbol{b}\nabla p) = \left(\boldsymbol{\Lambda} + \frac{1}{Q^*r}\boldsymbol{I}\right)\boldsymbol{Z}^{-1}\underline{\boldsymbol{N}} \tag{15}$$

Noting that the ith row of $\boldsymbol{Z}^{-1}$ is the ith eigenrow of $\boldsymbol{B}$, we can write the ith equation in Eq. 15 in the form

$$-\frac{1}{RT}(\boldsymbol{y}_i^T\boldsymbol{A}\nabla\boldsymbol{p} + \boldsymbol{y}_i^T\boldsymbol{b}\nabla p) = \left(\lambda_i + \frac{1}{Q^*r}\right)\boldsymbol{y}_i^T\underline{\boldsymbol{N}} \tag{16}$$

Let λ_1 be the zero eigenvalue of the positive semidefinite matrix $\boldsymbol{B}$ (Sotirchos and Burganos, 1988) and z_1 and $\boldsymbol{y}_1$ denote the corresponding eigenvector and eigenrow. By inspection of $\boldsymbol{B}$, one may readily see that

$$\boldsymbol{y}_1 = \left[\frac{1}{\alpha_i};\ i = 1, \ldots, n\right]^T \tag{17}$$

$$z_1 = x/\sum_j \frac{x_j}{\alpha_j} \tag{18}$$

Using Eqs. 17, 18, and 14, one may prove that

$$\boldsymbol{y}_1^T\boldsymbol{A}\nabla\boldsymbol{p} = \nabla\sum_j p_j = \nabla p \tag{19}$$

$$\boldsymbol{y}_1^T\boldsymbol{b} = \frac{Bp}{\mu}\sum_j \frac{x_j}{D_{Kj}};\ \boldsymbol{y}_i^T\boldsymbol{b} = 0,\ i \neq 1 \tag{20a, b}$$

Introducing Eqs. 19 and 20 in Eq. 16 gives

$$-\frac{1}{RT}\left(1 + \frac{Bp}{\mu}\sum_j \frac{x_j}{D_{Kj}}\right)\boldsymbol{y}_1^T\boldsymbol{A}\nabla\boldsymbol{p} = \frac{1}{Q^*r}\boldsymbol{y}_1^T\underline{\boldsymbol{N}} \tag{21}$$

$$-\frac{1}{RT}\boldsymbol{y}_i^T\boldsymbol{A}\nabla\boldsymbol{p} = \left(\lambda_i + \frac{1}{Q^*r}\right)\boldsymbol{y}_i^T\underline{\boldsymbol{N}},\ i \neq 1 \tag{22}$$

Eqs. 21 and 22 may also be written as

$$-\frac{1}{RT}D_i(\boldsymbol{y}_i^T\boldsymbol{A}\nabla\boldsymbol{p}) = \boldsymbol{y}_i^T\underline{\boldsymbol{N}},\ i = 1, \ldots n \tag{23}$$

with

$$D_1 = Q^*r + \frac{Bp}{\mu}\sum_j \frac{x_j}{\alpha_j};\ D_i = \left(\lambda_i + \frac{1}{Q^*r}\right)^{-1},\ i \neq 1 \tag{24a, b}$$

Eqs. 23 represent n independent single species diffusion problems for n pseudospecies, whose pressure gradients and fluxes are linear, pore size independent combinations of the pressure gradients and fluxes of the actual species. To be more specific, the pressure gradients are $\boldsymbol{y}_i^T\boldsymbol{A}\nabla\boldsymbol{P}$, the fluxes are $\boldsymbol{y}_i^T\underline{\boldsymbol{N}}$, and the diffusion coefficients are given by Eq. 24. For $i \neq 1$, the diffusion equations for the pseudospecies are identical to those used by Sotirchos and Burganos (1988) in the analysis of the isobaric problem. Note that the equation obtained from Eq. 23 for $i = 1$ and $\nabla p = 0$ is nothing else but Graham's law for isobaric diffusion, i.e.,

$$\boldsymbol{y}_1^T\underline{\boldsymbol{N}} = \frac{\underline{N}_j}{\alpha_j} = 0 \tag{25}$$

Equation 23 may be averaged over the population of pores in the capillary structure by employing the procedures discussed in my previous papers (Burganos and Sotirchos, 1987; Sotirchos and Burganos, 1988). Application of these procedures and orientational averaging (to induce isotropy to a possibly anisotropic pore structure) leads to the flux model

$$-\frac{1}{RT}D_{ie}^{S\text{ or }E\text{-}S}(\boldsymbol{y}_i^T\boldsymbol{A}\nabla\boldsymbol{p}) = \boldsymbol{y}_i^T\underline{\boldsymbol{N}},\ i = 1, \ldots n \tag{26}$$

or in matrix form

$$-\frac{1}{RT}\nabla p = \boldsymbol{A}^{-1}\boldsymbol{Z}(\boldsymbol{D}_e^{S\text{ or }E-S})^{-1}\boldsymbol{Z}^{-1}\underline{\boldsymbol{N}} \tag{27}$$

with

$$\boldsymbol{D}_e^{S\text{ or }E-S} = \mathbf{diag}\,(D_{ie}^{S\text{ or }E-S};\ i = 1, \ldots n) \tag{28}$$

Superscript S is used to denote the effective diffusion coefficients for the pseudospecies obtained when the smooth field approximation is directly applied to the original network. Superscript $E-S$, on the other hand, denotes the effective diffusion coefficients obtained when the smooth field approximation is applied to the effective network that results from application of the effective medium approximation (Kirkpatrick, 1973) to the original network. We have that (see Sotirchos and Burganos, 1988)

$$D_{ie}^{S\text{ or }E-S} = \frac{K}{3}\left(\left\langle l^2\frac{\pi r^2}{l}D_i\right\rangle_a \text{ or } \left\langle l^2\right\rangle_a\left\langle\frac{\pi r^2}{l}D_i\right\rangle_e\right) \tag{29}$$

K is the number of pores per unit volume, l is the pore length, and the symbols $\langle\bullet\rangle_a$ and $\langle\bullet\rangle_e$ are employed to indicate the arithmetic average and effective medium average values of quantity $\bullet$, respectively. The effective medium average for some quantity, say q, with number distribution density $f(q)$ is obtained from the solution of the equation (Kirkpatrick, 1973)

$$\int_q \frac{q-\langle q\rangle_e}{q+\left(\frac{z}{2}-1\right)\langle q\rangle_e} f(q)\,dq = 0 \tag{30}$$

z is the coordination number of the network, that is, the average number of pores emanating from a site. For networks of pores of uniform length, Eq. 29 becomes

$$D_{ie}^{S\text{ or }E-S} = \frac{\epsilon}{3}\frac{\langle D_i r^2\rangle_{a\text{ or }e}}{\langle r^2\rangle_a} \tag{31}$$

In contrast to the flux models derived through the Feng and Stewart procedure (as discussed previously), the flux models constructed here require the computation of n average quantities only for each set of pressure and composition values. Nevertheless, the computation of these averages requires that the eigenvalues and eigenvectors of matrix $\boldsymbol{B}$ be available, which, like the matrix elements, F_{ij}, in the Feng and Stewart model, can be computed analytically only for multicomponent mixtures of a few species. The real advantage of the class of flux models that I have developed here is that the decomposed equations (Eq. 23) can be integrated over the pore size and orientation distributions using any applicable procedure. Moreover, as we shall see in the next section, the particular form of Eqs. 26 and 27 lends itself to a direct comparison with the "three-parameter" dusty-gas model for nonisobaric diffusion. It should be pointed out that despite its different algebraic form, the flux model derived through application of the SFA procedure (Eqs. 27 and 29, superscript S) is identical to the Feng and Stewart flux model (Eqs. 9 and 10).

Figure 1 presents the variation of the ratio of effective diffusivities, D_{1e}^{E-S} and D_{1e}^{S}, with the population ratio, f_1/f_2, of a discrete, bimodal pore structure, with f_i being the number of pores of radius r_i per unit volume. The results of Figure 1 have been parametrized using the coordination number of the network, z, and parameter γ, which is defined as $\gamma = p/8\mu\Sigma_j(x_j/\alpha_j)r_2$. γ determines whether mass transport in the presence of total pressure gradients occurs in the Knudsen flow regimen ($\gamma \to 0$), the viscous flow regimen ($\gamma \to \infty$), or in the intermediate transition regime. It is seen that the EMT-SFA procedure predicts much lower values for the effective transport coefficient, D_{1e}, in a wide range of values of population ratio, by more than three orders of magnitude in some cases. Such behavior is expected since, when the smooth field approximation is directly applied to the original network, the estimated effective transport coefficient reflects an *in parallel* combination of the transport resistances of the pores, and consequently, it offers an upper bound on the actual effective transport coefficient. The SFA effective transport coefficient is in a way equivalent to the upper bound obtained when variational formulation of the transport problem in certain porous media with a linear trial function is used (e.g., Strieder and Aris, 1973; Faley and Strieder, 1987).

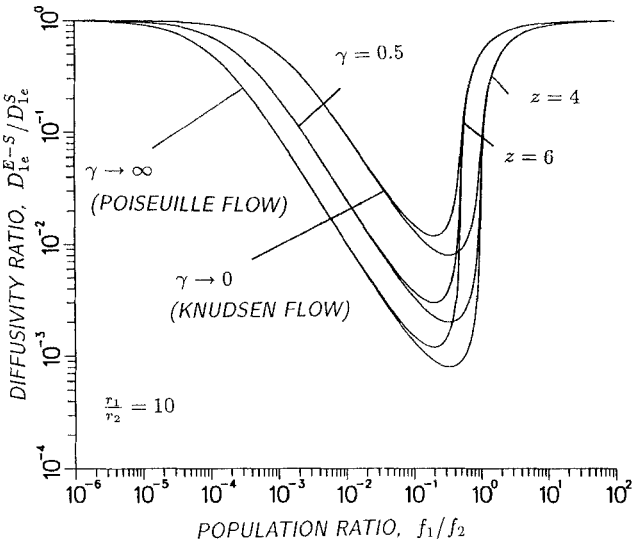

Figure 1. Variation of the D_{1e}^{E-S}/D_{1e}^{S} ratio with the population ratio of a discrete, bimodal pore system.

$\gamma = \frac{p}{8\mu}\sum_j \frac{x_j}{\alpha_j} r_2$.

The ratio of the EMT-SFA and SFA effective transport coefficients, D_{1e}^{E-S}/D_{1e}^{S}, approaches unity as the pore system tends to become unimodal, that is, for small and large values of the population ratio. For the same reason, the relative difference between the two effective diffusivities diminishes as the radius ratio of the bimodal pore system decreases and the distribution becomes narrower. As the results of Figure 1 show, increasing the coordination number also leads to smaller differences between the SFA and EMT-SFA estimates of transport coeffcient, D_{1e}. Larger coordination numbers imply a higher degree of crosslinking among the pores of the network, and thus the actual network gets closer to the situation of *perfect crosslinking*, that is tacitly assumed when the smooth field approximation is invoked.

The largest relative difference between D_{1e}^{E-S} and D_{1e}^{S} occurs

in the vicinity of the percolation threshold of the network, predicted to be equal to $2/(z-2)$ by the effective medium theory; namely, $(f_1/f_2)_p = 1$ for $z = 4$ and $(f_1/f_2)_p = 0.5$ for $z = 6$. For values of population ratio sufficiently lower than the percolation threshold, the diffusivity ratio appears to be independent of the coordination number, z. This behavior is primarily due to the fact that below the percolation threshold, the effective medium average $\langle D_1(r)r^2\rangle e$ is almost equal to $D_1(r_2)r_2^2$ and, hence, independent of the coordination number. For population ratios sufficiently larger than the percolation threshold, on the other hand, $\langle D_1(r)r^2\rangle_e$ and $\langle D_1(r)r^2\rangle_a$ are almost proportional to $D_1(r_1)r_1^2\rangle$, with the proportionality constant being determined by the coordination number and the population ratio for the effective medium average and by the population ratio for the arithmetic average. As a result, D_{1e}^{E-S}/D_{1e}^{S} (or equivalently, $\langle D_1(r)r^2\rangle_e/\langle D_1(r)r^2\rangle_a$) turns out to be almost independent of the value of parameter γ above the percolation threshold.

The variation of the D_{ie}^{E-S}/D_{ie}^{S} ratio ($i \neq 1$) with the population ratio, shown in Figure 2, is qualitatively similar to that seen in Figure 1 for $i = 1$. The results of Figure 2 have been parametrized using the coordination number z and parameter β defined as $\beta = \lambda_i Q^* r_2$. β determines whether diffusion occurs in the Knudsen regime ($\beta \to 0$), the molecular diffusion regime ($\beta \to \infty$), or the intermediate transition regime. The only noteworthy difference between the results of Figures 1 and 2 is that, for $i = 1$ (Figure 1), the relative difference between SFA and EMT-SFA transport coefficients is larger. Again, the largest relative differences are encountered in the vicinity of the percolation threshold of the network. It should be pointed out that the effects of β and γ on effective diffusion coefficients D_{ie}^{E-S} and D_{ie}^{S}, as inferred from Figures 1 and 2, were also observed by Nicholson and Petropoulos (1977, 1978) in their analysis of binary mass transport in the special cases of serial (EMT-SFA for $z = 2$) or parallel (SFA or EMT-SFA for $z = \infty$) arrangements of cylindrical capillaries.

Results on the difference of the predictions of the SFA and EMT-SFA flux models for continuous, unimodal pore-size distributions are given in Figures 3 and 4 for $i = 1$ and $i \neq 1$, respectively. Gaussian and uniform pore-size distribution densities for the porosity density function, $\epsilon(r)$, were used to get the results of Figures 3 and 4. Since uniform pore length and no pore overlap is considered in this particular application, the population density functions needed to compute the effective medium and arithmetic averages appearing in the expression for D_{ie} are obtained by dividing $\epsilon(r)$ by r^2. The dimensionless variance of the porosity density functions σ/r_m has been used as abscissa in the presentation of the results in Figures 3 and 4, with r_m being the mean of the pore-size distribution. Results for the Gaussian pore-size distribution extend up to $\sigma/r_m = 0.25$ because the

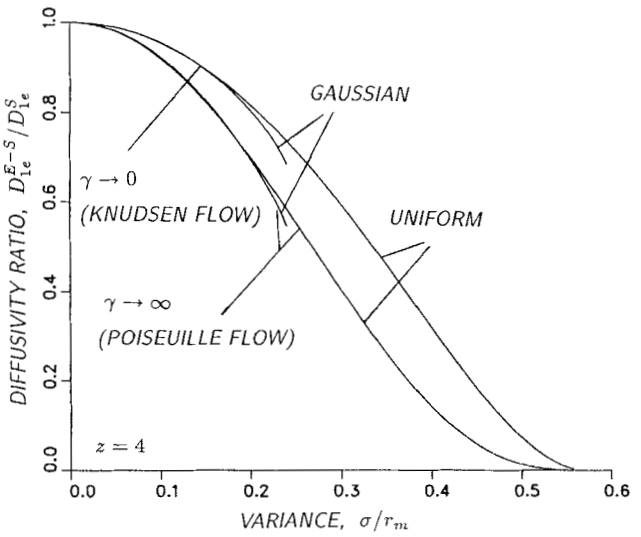

Figure 3. Variation of the D_{1e}^{E-S}/D_{1e}^{S} ratio with the relative variance for Gaussian and uniform pore-size distributions.

r_m is the mean of the distribution, and $\gamma = p/8\mu \Sigma_j x_j/\alpha_j r_m$.

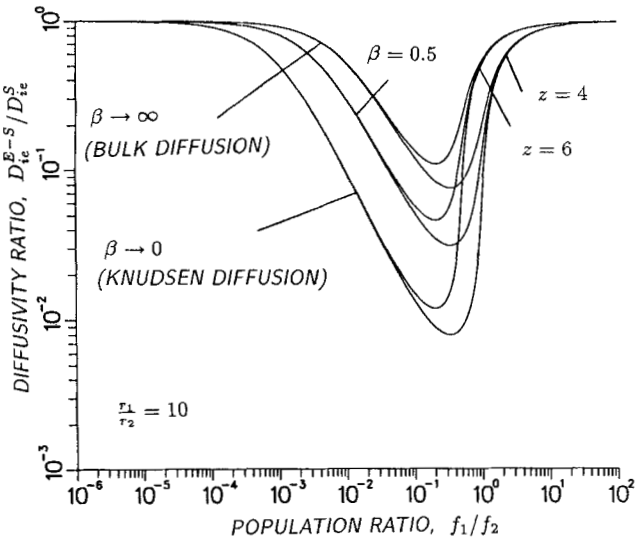

Figure 2. Variation of the D_{ie}^{E-S}/D_{ie}^{S} ratio ($i \neq 1$) with the population ratio of a discrete, bimodal pore system.

$\beta = \lambda_i Q^* r_2$.

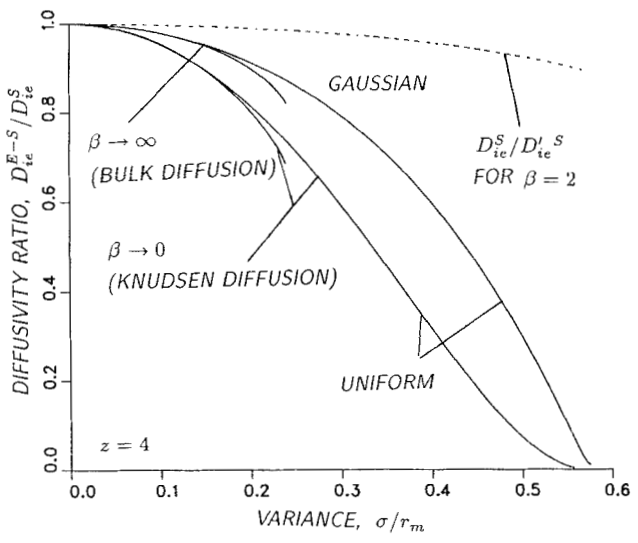

Figure 4. Variation of the D_{ie}^{E-S}/D_{ie}^{S} ratio with the relative variance for Gaussian and uniform pore-size distributions.

r_m is the mean of the distribution, and $\beta = \lambda_i Q^* r_m$.

numerically important part of the distribution was assumed to extend over the range $[r_m - 4\sigma, r_m + 4\sigma]$. For the uniform pore-size distribution the results shown extend up to $\sigma/r_m = 1/\sqrt{3}$, a value corresponding to the point where the lower limit of the uniform pore-size distribution becomes zero.

It is seen in the results of Figures 3 and 4 that the EMT-SFA model predicts lower effective values for the transport coefficients that the SFA model, with the relative differences being again larger for $i = 1$. However, the predicted relative differences for unimodal pore-size distributions are much lower than those for bimodal systems. (Compare the results of Figures 1 and 2 with those of Figures 3 and 4.) Similar observations were also made by Nicholson and Petropoulos (1973) in their study of transport of dilute gases in serial or parallel networks of capillaries. The D_{ie}^{E-S}/D_{ie}^{S} ratio deviates more from unity as the variance increases and the distribution become broader. For small variance values, the results for the diffusivity ratio appear to be independent of the type of the porosity density function. As in the case of bimodal pore-size distribution, the observed differences between EMT-SFA and SFA estimates decrease with increasing coordination number, with the diffusivity ratio approaching unity for all σ/r_m values as the coordination number increases without limit.

Comparison of the SFA and EMT-SFA Nonisobaric Flux Models with the "Three-Parameter" Dusty-Gas Model

The SFA and EMT-SFA procedures can be used to derive expressions for the three parameters of the dusty-gas model in a rather straightforward fashion provided that some simplifying assumptions are made as follows.

- The diffusive and convective contributions of the fluxes can be integrated independently over the pore population—an obviously true assumption if the smooth field approximation is directly applied to the original network, as discussed earlier.
- The partial pressure gradients can be viewed as made up of separate, additive contributions for Knudsen and molecular diffusion, which again can be treated independently.

Following a procedure described in my previous paper (Sotirchos and Burganos, 1988), it can be shown that for a uniform pore length network, the three parameters of the dusty-gas model are given by the following expressions:

$$\mathcal{D}_{ij,e}^{S\text{ or }E-S} = \frac{\epsilon}{3}\mathcal{D}_{ij}\frac{\langle r^2\rangle_{a\text{ or }e}}{\langle r^2\rangle_a} \tag{32}$$

$$D_{Ki,e}^{S\text{ or }E-S} = \frac{\epsilon}{3}Q_i\frac{\langle r^3\rangle_{a\text{ or }e}}{\langle r^2\rangle_a} \tag{33}$$

$$B_e^{S\text{ or }E-S} = \frac{\epsilon}{24}\frac{\langle r^4\rangle_{a\text{ or }e}}{\langle r^2\rangle_a} \tag{34}$$

Similar equations (compare Eqs. 29 and 31) hold for the more general case of distributed length pore networks.

The "three-parameter" dusty-gas model with parameters given by Eqs. 32–34 can be recast in a form similar to that of the general flux model (Eq. 27). Using the procedure followed for the dusty-gas model equations for a single pore (Eqs. 11–23), we get after some rearrangement

$$-\frac{1}{RT}\nabla p = \boldsymbol{A}^{-1}\boldsymbol{Z}(\boldsymbol{D}_e'^{\,S\text{ or }E-S})^{-1}\boldsymbol{Z}^{-1}\underline{\boldsymbol{N}} \tag{35}$$

where the elements of the diagonal matrix $\boldsymbol{D}_e'^{\,S\text{ or }E-S}$ are given by

$$D_{ie}'^{\,S\text{ or }E-S} = \frac{\epsilon}{3\langle r^2\rangle_a}\left(\frac{\lambda_i}{\langle r^2\rangle_{a\text{ or }e}} + \frac{1}{Q^*\langle r^3\rangle_{a\text{ or }e}}\right)^{-1}, i \neq 1 \tag{36}$$

$$D_{1e}'^{\,S\text{ or }E-S} = \frac{\epsilon}{3\langle r^2\rangle_a}\left(Q^*\langle r^3\rangle_{a\text{ or }e} + \frac{p}{8\mu}\sum_j\frac{x_j}{\alpha_j}\langle r^4\rangle_{a\text{ or }e}\right) \tag{37}$$

It is readily seen by comparing Eqs. 27 and 35 that the accuracy of the predictions of the "three-parameter" dusty-gas model with parameters given by Eqs. 32–34 is solely determined by the error involved in the approximation of $D_{ie}^{S\text{ or }E-S}$ by $D_{ie}'^{\,S\text{ or }E-S}$. Using Eqs. 24, 31, 36 and 37, one finds that the approximations involved are

$$\left\langle\frac{1}{\frac{\lambda_i}{r^2} + \frac{1}{Q^*r^3}}\right\rangle_{a\text{ or }e} \simeq \frac{1}{\frac{\lambda_i}{\langle r^2\rangle_{a\text{ or }e}} + \frac{1}{Q^*\langle r^3\rangle_{a\text{ or }e}}}, i \neq 1 \tag{38}$$

and

$$\left\langle Q^*r^3 + \frac{p}{8\mu}\sum_j\frac{x_j}{\alpha_j}r^4\right\rangle_{a\text{ or }e} \simeq \left(Q^*\langle r^3\rangle_{a\text{ or }e} + \frac{p}{8\mu}\sum_j\frac{x_j}{\alpha_j}\langle r^4\rangle_{a\text{ or }e}\right) \tag{39}$$

The approximation described by Eq. 38 is the same as that involved in the isobaric diffusion problem. Calculations for a discrete, bimodal pore-size distribution with $r_1/r_2 = 10$ in my previous paper (Sotirchos and Burganos, 1988) showed that the error involved was rather small in the most part of the space of porosity and pore size ratios. Obviously, the approximation is exact in the limiting regimes of Knudsen and molecular diffusion ($\lambda_i Q^* r \ll 1$ and $\lambda_i Q^* r \gg 1$, respectively) or for pore structures of uniform pore size. The additional approximation that has to be considered in the case of nonisobaric diffusion is that given by Eq. 39. Since the arithmetic average (subscript a) is a linear functional, the approximation described by Eq. 39 is exact if the smooth field approximation (SFA procedure) is applied directly to the pore network. This result has been expected because of the additivity of viscous and diffusive fluxes assumed in the construction of the dusty-gas model equations for a single pore. The effective medium average, however, is a nonlinear functional, and hence the error involved in the approximation of Eq. 39 has to be investigated.

Figure 5 presents the variation of the diffusivity ratio $D_{1e}'^{\,E-S}/D_{1e}^{E-S}$ ratio with the population ratio for a bimodal pore-size distribution for various ratios of pore radius. It is seen that $D_{1e}'^{\,E-S}/D_{1e}^{E-S}$ deviates significantly from unity only in a very small interval of the range of population ratio (note the scale of the x-axis of the graph). The size of this interval decreases with increasing pore size ratio, but the maximum relative deviation increases. At the limit of infinitely large pore size ratio, the rela-

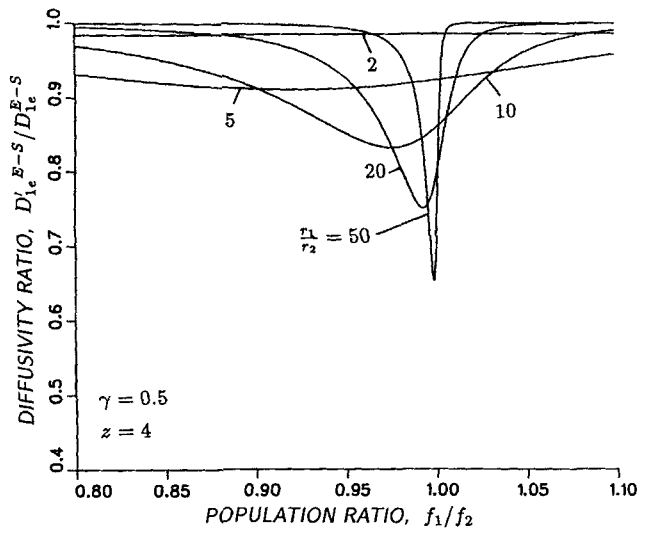

Figure 5. Variation of the $D'^{E-S}_{1e}/D^{E-S}_{1e}$ ratio with the population ratio of a discrete, bimodal pore system.

tive difference between the two diffusivities also becomes infinitely large, while the interval at which it is observed becomes infinitesimally small. The population ratio value at which $D'^{E-S}_{1e}/D^{E-S}_{1e}$ attains its minimum approaches the percolation threshold of the network from below with increasing pore size ratio. The difference between the effective transport coefficient predicted by the rigorous EMT-SFA flux model and that obtained using its "three-parameter" counterpart approaches zero as the coordination number of the network increases, since the approximation of Eq. 39 is exact for $z = \infty$ (SFA model). It should be pointed out that the value of γ used to obtain the results of Figure 5 lies within the range in which the largest differences were observed.

The variation of the $D^{E-S}_{ie}/D'^{E-S}_{ie}$ (for $i \neq 1$) ratio with the population ratio for various pore size ratios is given in Figure 6.

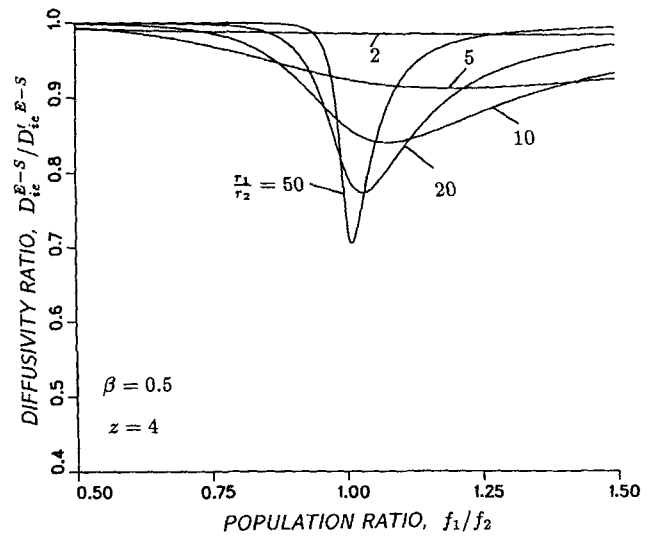

Figure 6. Variation of the $D^{E-S}_{ie}/D'^{E-S}_{ie}$ ratio with the population ratio of a discrete, bimodal pore system.

The behavior of the curves of Figure 6 is, in general, qualitatively similar to that of those of Figure 5. The most noteworthy differences between the results of Figures 5 and 6 are that in the latter:

a) It is the "three-parameter" approximation that predicts larger transport coefficients.

b) Significant deviations between the rigorous and approximate coefficients are observed over a wider interval of population ratio.

c) The minimum diffusivity ratio values are higher.

d) With increasing pore size ratio the f_1/f_2 value at which the minimum occurs approaches the percolation threshold from above.

The β value used to get the results of Figure 6 lies, like that of γ in Figure 5, near the value where the largest relative differences were observed.

Figure 7 gives the variation of the D^S_{ie}/D'^S_{ie} ratio (SFA flux model) with the porosity ratio ϵ_1/ϵ_2 [$\epsilon_1/\epsilon_2 = (f_1/f_2)(r_1/r_2)^2$]. It can be shown that, for a given r_1/r_2 ratio, D^S_{ie}/D'^S_{ie} attains its minimum for $\beta = \epsilon_1/\epsilon_2 = \sqrt{r_2/r_1}$. (At the minimum, $D^S_{ie}/D'^S_{ie} = 4/[2 + \sqrt{r_1/r_2} + \sqrt{r_1/r_2}]$.) Unlike the approximations discussed for the results of Figures 5 and 6, the approximation of Figure 7 tends to present much larger deviations extending over relatively large intervals of porosity ratio (or equivalently, population ratio) values. The D^S_{ie}/D'^S_{ie} ratio was found to deviate noticeably from unity even for unimodal pore size distributions (see the dashed curve in Figure 4). On the contrary, for the Gaussian and uniform pore-size distributions used to obtain the results of Figure 4, the maximum deviation from unity that could be found for $z = 4$ was less than 1.5% for $D'^{E-S}_{1e}/D^{E-S}_{1e}$, while $D^{E-S}_{ie}/D'^{E-S}_{ie}$ ($i \neq 1$) was practically unity over the whole range of relative variance. Since the results of Figure 7 could also be obtained using the EMT-SFA procedure for $z = \infty$, one concludes by comparing Figures 6 and 7 that the relative difference between D^{E-S}_{ie} and D'^{E-S}_{ie} for $i \neq 1$ would increase with increasing coordination number.

Some computational results obtained by applying the four flux models to the problem of convection and diffusion in a dis-

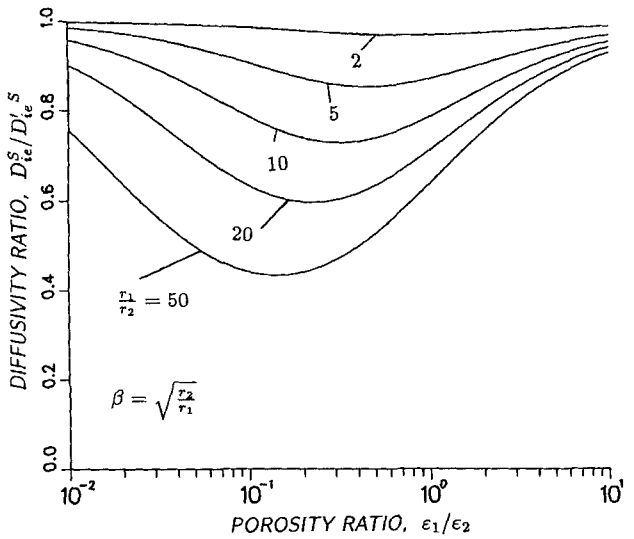

Figure 7. Variation of the D^S_{ie}/D'^S_{ie} ratio with the porosity of a discrete, bimodal pore system. $f_1/f_2 = (\epsilon_1/\epsilon_2)(r_2/r_1)^2$.

crete, bimodal pore structure of an equimolar, quaternary mixture of CO_2, CO, H_2, and CH_4, are presented in Table 1. The conditions used were 1,000 K temperature and 1 atm total pressure. The partial pressure gradients were assumed to be colinear and to satisfy the relationships $\nabla p_{CO_2} = \nabla p_{H_2} = \nabla p$ and $\nabla p_{CO} = \nabla p_{CH_4} = -0.5\nabla p$, with ∇p being the total pressure gradient. The Chapman-Enskog theory (Bird et al., 1960) was used to compute the binary diffusion coefficients and the viscosities of the gaseous species, while the viscosity of the mixture ($\mu = 3.629 \times 10^{-5}$ kg/m · s at the above conditions) was determined using the semiempirical Wilke equation described in the above reference. The values for the effective transport coefficients and mass transport fluxes that are reported in Table 1 were rendered independent of the total porosity and total pressure gradient by dividing their values by ϵ and $\epsilon\nabla p$, respectively.

The results of Table 1 for $r_1 = 0.2$ μm and $r_2 = 0.02$ μm show that the rigorous EMT-SFA model predicts effective transport coefficients and fluxes that are practically identical to those of the corresponding "three-parameter" dusty-gas model. In view of the results seen in Figures 5 and 6, such a behavior is not surprising since the porosity ratio used in Table 1 is far from the percolation threshold of the pore network [$(\epsilon_1/\epsilon_2)_p = 0.01$]. In contrast to the EMT-SFA estimates, there are noticeable differences between the predictions of the rigorous SFA model and those of its "three-parameter" version, which, however, are considerably smaller than those seen between the EMT-SFA and SFA results. In accordance with the results of Figure 7, the approximate SFA model is found to predict higher effective transport coefficients. The behavior of the results for $r_1 = 2$ μm and $r_2 = 0.2$ μm is qualitatively similar to that for the smaller radius values, the main difference being that effective transport coefficient for the first pseudospecies (which accounts for convection) is considerably larger than the other transport coefficients, by a factor of 2 for the EMT-SFA flux model and by a factor of 10 for the SFA flux model. This indicates that convection is the prevailing model of mass transport for the larger radius solid, especially for the SFA flux model. Indeed, note that both versions of the SFA model predict net flow for all species in the direction of the total pressure gradient, that is CO and CH_4 appear to be transported against their own partial pressure gradient. Since the effective transport coefficient for convection (subscript 1) is computed exactly in the "three-parameter" version of the dusty gas model, the relative differences between rigorous and approximate SFA predictions are lower in the case of the larger pores solid.

It should be noted that for pore-size distributions of realistic breadth (i.e., $r_1/r_2 < 10$), the observed maximum differences between the effective transport coefficients predicted by the rigorous SFA and EMT-SFA flux models and the corresponding "three-parameter" dusty-gas models are seldom above 30%, much smaller than the deviations that exist between the SFA and EMT-SFA extimates. Another interesting observation is that, for the EMT-SFA results, the largest differences are encountered in the vicinity of the percolation threshold. Since the rigorous EMT-SFA effective transport coefficient was found to deviate noticeably near the percolation threshold from the exact effective transport coefficient, as determined by direct solution of the transport equation in a statically representative sample of the network (Burganos and Sotirchos, 1987), one cannot say *a priori* whether D_{ie}^{E-S} or $D_{ie}^{\prime E-S}$ will be closer to the exact result there. In view of the observations, I believe that the approximation of the rigorous EMT-SFA and SFA transport coefficients by the "three-parameter" flux models must be considered satisfactory. This provides a partial explanation as to why the "three-parameter" dusty-gas model has been successful in correlating mass transport data even for heteroporous solids (Chen and Rinker, 1979; Mason and Malinauskas, 1983). Use of the "three-parameter" versions in mathematical models becomes particularly attractive when one considers the immense computational effort that is required for implementation of the rigorous EMT-SFA and SFA flux models.

Summary and Conclusions

A general method was developed in this study for treating the problem of multicomponent diffusion and convection in capillary structures, with the objecting of developing flux models for nonisobaric diffusion in such structures. The development of the method was based on the extension of an Eigenvector-Eigenvalue decomposition of the dusty-gas models equations, introduced in a previous paper (Sotirchos and Burganos, 1988) for isobaric diffusion. The method was used to construct flux models for multicomponent diffusion and convection by assuming microscopically smooth partial pressure fields in the original pore network (SFA flux model) or in the equivalent network that results when the effective medium theory for resistor net-

Table 1. Effective Transport Coefficients and Mass-Transport Fluxes for an Equimolar, Quaternary Mixture in a Bimodal Pore Structure*

	Eff. Diffusivities $\times 10^5$, D_{ie}/ϵ (m^2/s)				Fluxes $\times 10^{12}$, $\underline{N}_i/(\epsilon\nabla p)$ (kmol·s/kg)			
	1	2	3	4	CO_2	CO	H_2	CH_4
$\tau_1 = 10\tau_2 = 0.2$ μm								
EMT-SFA	0.16024	0.14930	0.14785	0.14902	−0.18398	0.10804	−0.84140	0.14117
$(EMT\text{-}SFA)_{app}$	0.16024	0.14930	0.14785	0.14902	−0.18398	0.10804	−0.84140	0.14117
SFA	1.8476	1.0910	1.0325	1.0791	−1.6348	0.48876	−6.3507	0.63255
$(SFA)_{app}$	1.8476	1.2593	1.2077	1.2489	−1.7628	0.69188	−7.2357	0.89028
$\tau_1 = 10\tau_2 = 2$ μm								
EMT-SFA	1.7434	0.97471	0.91590	0.96270	−1.5004	0.39538	−5.7014	0.51036
$(EMT\text{-}SFA)_{app}$	1.7434	0.97471	0.91590	0.96270	−1.5004	0.39539	−5.7014	0.51037
SFA	32.296	3.0624	2.7396	2.9933	−16.996	−11.074	−29.928	−10.990
$(SFA)_{app}$	32.296	3.8047	3.3698	3.7117	−17.498	−10.148	−33.502	−10.113

*$\nabla p_{CO_2} = \nabla p_{H_2} = \nabla p$; $\nabla p_{CO} = \nabla p_{CH_4} = -0.5\,\nabla p$; $z = 4$; $\epsilon_1/\epsilon_2 = 1$

works is applied to the original network (EMT-SFA flux model). For a multicomponent mixture of n species, each flux model involves n effective mass transport coefficients.

The special structure of the developed flux models permitted their direct comparison with the "three-parameter" dusty-gas model for porous solids, in which effective values are employed for the binary and Knudsen diffusivities and the permeability of the porous medium. Computations for discrete and continuous distributions of pore size revealed small differences between the predictions of the flux models constructed in this study and those of the "three-parameter" dusty-gas model, provided that the same procedure (i.e., SFA or EMT-SFA) is used to obtain estimates for its three parameters. Very large differences, by more than some orders of magnitude for small coordination numbers, were found to exist between the effective mass transport coefficients estimated by the EMT-SFA and SFA flux models, with the SFA coefficients being the larger. These differences were found to diminish with increasing coordination number and decreasing variance of the pore-size distribution. Depending on the relative importance of convective and diffusive transport, the predictions of the SFA and EMT-SFA flux models may differ both quantitatively and qualitatively. For instance, computations for a quarternary mixture showed that, under conditions of significant convective contribution in the fluxes, the two models may predict net flow for some of the species of the mixture in opposite directions.

Acknowledgment

This research was supported by a grant from the U.S. Department of Energy.

Notation

$\boldsymbol{A}$ = diagonal matrix defined in Eq. 12
$\boldsymbol{B}$ = matrix defined in Eqs. 11 and 14
B, B_e = permeability of a pore and effective permeability, respectively, m^2
$\boldsymbol{D}_e$ = diagonal matrix of the effective diffusivities for the pseudospecies
D_{ie} = effective transport coefficient of pseudospecies i, m^2/s
$\mathcal{D}_{ij}, \mathcal{D}_{ij,e}$ = binary diffusivity of the (i,j) pair and effective binary diffusivity, respectively, m^2/s
$D_{Ki}, D_{Ki,e}$ = Knudsen diffusivity of species i in a pore and effective Knudsen diffusivity of species i, respectively, m^2/s
$f(r)dr$ = number of pores per unit volume with radius in the range $[r, r + dr]$, m^{-3}
f_i = number of pores per unit volume with conductance r_i in a network with discrete distribution of pore size, m^{-3}
K = total number of pores per unit volume, m^{-3}
l = length of a pore, m
M_i = molecular weight of species i, kg/kmol
n = number of species in the mixture
$\underline{n}_k$ = unit vector parallel to the axis of pore k
$\underline{\bar{N}}$ = vector of diffusion fluxes
$\underline{\bar{N}}_i$ = diffusion flux of species i, kmol/m^2 · s
p = total pressure of the mixture, Pa
p_i = partial pressure of species i, Pa
$\boldsymbol{p}$ = vector of partial pressures
Q_i = Knudsen proportionality constant for species i (see eq. 2a), m/s
Q^* = reference value for Q_i, m/s
R = ideal gas law constant, J/kmol · K
r = pore radius, m
S_i = parameters defined in Eq. 6
T = temperature, K
x_i = mole fraction of species i
$\mathbf{x}$ = vector of mole fractions
z = coordination number
$\boldsymbol{Z}$ = matrix of eigenvectors of matrix $\boldsymbol{B}$

Greek letters

α_i = dimensionless Knudsen proportionality constant for species i, $= Q_i/Q^*$
β = parameter defined as $\beta = \lambda_1 Q^* r^*$, where r^* is a reference value for the pore radius
γ = parameter defined as $\gamma = p/8\mu \sum_j x_i/\alpha_i r^*$
∇p_i = partial pressure gradient for species i, Pa/m
∇p = total pressure gradient, Pa/m
ϵ = porosity
$\epsilon(r)dr$ = porosity of pores with radius in the range $[r, r + dr]$
ϵ_i = porosity of pores of radius r_i in a network with discrete distribution of pore size
λ_i = ith eigenvalue of matrix $\boldsymbol{B}$, s/m^2
λ_1 = zero eigenvalue of matrix $\boldsymbol{B}$, s/m^2
$\boldsymbol{\Lambda}$ = diagonal matrix of the eigenvalues of $\boldsymbol{B}$
μ = viscosity of the gaseous mixture, kg/m · s

Subscripts

e = effective quantities
i = quantities referring to species i, pseudospecies i, or ith pore size of a discrete pore-size distribution

Superscripts

$E-S$ = quantities obtained using the EMT-SFA method
S = quantities obtained using the SFA method

Symbols

$\langle \bullet \rangle_a$ = arithmetic average value of quantity $\bullet$
$\langle \bullet \rangle_e$ = effective medium average value of quantity $\bullet$

Literature Cited

Bird, R. B., W. E. Stewart, and E. N. Lightfoot, *Transport Phenomena*, Wiley, New York (1960).

Burganos, V. N., and S. V. Sotirchos, "Diffusion in Pore Networks. Effective Medium Theory and Smooth Field Approximation," *AIChE J.*, **33**, 1678 (1987).

Chen, O. T., and R. G. Rinker, "Modification of the Dusty-Gas Equation to Predict Mass Transfer in General Porous Media," *Chem. Eng. Sci.*, **34**, 51 (1979).

Deriagin, B. V., and S. P. Bakanov, "Theory of the Flow of a Gas in a Porous Material in the Near-Knudsen Region," *Tech. Phys.*, **2**, 1904 (1957).

Faley, T. L., and W. Strieder, "Knudsen Flow through a Random Bed of Unidirectional Fibers," *J. Appl. Phys.*, **62**, 4394 (1987).

Feng, C., and W. E. Stewart, "Practical Models for Isothermal Diffusion and Flow of Gases in Porous Solids," *Ind. Eng. Chem. Fund.*, **12**, 143 (1973).

Froment, G. F., and K. B. Bischoff, *Chemical Reactor Analysis and Design*, Wiley, New York (1979).

Jackson R., *Transport in Porous Catalysts*, Elsevier, Amsterdam (1977).

Johnson, M. F. L., and W. E. Stewart, "Pore Structure and Gaseous Diffusion in Solid Catalysts," *J. Cat.*, **4**, 248 (1965).

Kirkpatrick, S., "Percolation and Conduction," *Rev. Mod. Phys.*, **45**, 574 (1973).

Mason, E. A., and A. P. Malinauskas, *Gas Transport in Porous Media: The Dusty-Gas Model*, Elsevier, New York (1983).

Mason, E. A., A. P. Malinauskas, and R. B. Evans III, "Flow and Diffusion of Gases in Porous Media," *J. Chem. Phys.*, **46**, 3199 (1967).

Nicholson, D., and J. H. Petropoulos, "Capillary Models for Porous Media: IV. Flow Properties of Parallel and Serial Capillary Models with Various Radius Distributions," *J. Phys. D: Appl. Phys.*, **6**, 1737 (1973).

——— "Capillary Models for Porous Media: VIII. Study of Gaseous Flow in the Transition from the Knudsen to the Poiseuille Flow Regimes," *J. Phys. D: Appl. Phys.*, **11**, 1179 (1978).

——— "Capillary Models for Porous Media: VII. Study of Gaseous Flow in the Transition from the Knudsen to the Counter-diffusion Regimes," *J. Phys. D: Appl. Phys.*, **11**, 1179 (1978).

Sotirchos, S. V., and V. N. Burganos, "Analysis of Multicomponent Diffusion in Pore Networks," *AIChE J.*, **34**, 1106 (1988).

Strieder, W., and R. Aris, *Variational Methods Applied to Problems of Diffusion and Reaction*, Springer-Verlag (1973).

Manuscript received July 24, 1989, and revision received Sept. 20, 1989.